First-order and higher-order interferences in the $^{15}C + ^{208}Pb$ and $^{11}Be + ^{208}Pb$ reactions

B. Mukeru* and M. L. Lekala†
Department of Physics, University of South Africa, P.O. Box 392, Pretoria 0003, South Africa
(Received 13 January 2015; revised manuscript received 4 March 2015; published 11 June 2015)

First-order and higher-order interferences effects on the total, Coulomb, and nuclear breakup cross sections in the $^{15}C + ^{208}Pb$ and $^{11}Be + ^{208}Pb$ reactions are studied at 68 MeV/u incident energy. A partial-wave analysis is first performed, and shows that the differential total breakup cross sections are dominated by the p waves. However, considered alone, they largely underestimate the data, hence the importance of the other partial-wave contributions. It is also shown that the first-order interference reduces by more than 60% the total breakup cross sections, by less than 3% the Coulomb breakup cross sections, and by more than 85% the nuclear breakup cross sections, for both reactions. On the other hand, the higher-order interferences are found to reduce by less than 9% the total breakup cross section, less than 1% the Coulomb breakup cross section, and less than 7% the nuclear breakup cross section for the $^{15}C + ^{208}Pb$ reaction. For the $^{11}Be + ^{208}Pb$ reaction however, the higher-order interference reduces by less than 7% the total breakup cross section, by less than 1% the Coulomb breakup cross section, and by less than 4% the nuclear breakup cross section. It is finally shown that even at first order, the incoherent sum of the nuclear breakup cross sections is more important than the incoherent sum of the Coulomb breakup cross sections for the two reactions.

DOI: 10.1103/PhysRevC.91.064609 PACS number(s): 24.10.Eq, 25.60.Dz, 25.60.Gc

I. INTRODUCTION

The Coulomb dissociation (CD) method based on the first-order approximation restricted to the $E1$ multipole [1–3], has been intensively used to study the structure of halo nuclei [4–10]. The $E1$ multipole restriction is mostly justified by the assumption that higher-order or non- first-order effects are negligible in the Coulomb breakup induced by a neutron-halo projectile [10,11]. In particular, it was shown in Ref. [7], that the higher-order multipole transitions reduce by less than 4% the overall Coulomb breakup cross section. However, this method has received criticisms regarding the elimination of the nuclear breakup contribution to keep only the pure Coulomb breakup cross section [12,13], in the sense that the scaling method mostly used to eliminate the nuclear breakup contribution [9,14], was found to not be always reliable due to the significance of the Coulomb-nuclear interference [12]. Various studies have also shown that a small nuclear contribution does not necessarily mean negligible Coulomb-nuclear interference [15–19], thus raising more issues in the exclusion of the nuclear breakup cross section.

Another argument put forward for the $E1$ transition restriction in the analysis of the $^{15}C + ^{208}Pb$ reaction was that all the outgoing neutrons are in the p waves and the breakup occurs in one step [20]. However, analyzing the same reaction in Ref. [21], using the CDCC (continuum discretized coupled channel) method [22,23], it was shown that all the outgoing neutrons are not in the p waves and that the multistep process plays an important role. While one could expect the Coulomb breakup cross section to fit the experimental data, the authors showed that the data are rather well fitted by the Coulomb+nuclear breakup cross section. However, it is not clear whether this is an exclusive effect of the Coulomb-nuclear interference.

Although the first- and higher-order interference effects have received considerable attention, these effects are not yet fully understood for both Coulomb+nuclear and nuclear breakup cross sections, and they could shed more light in the understanding of the role of the nuclear breakup in a Coulomb dominated reaction, induced by a neutron-halo projectile.

For reactions induced by the proton-halo nucleus ^{8}B, it was shown in Refs. [24,25] that, for the Coulomb+nuclear breakup cross section, the different multipole interference plays a rather important role, and is strongly destructive. In Ref. [26], for example, where both Coulomb and nuclear breakups were considered separately, the authors obtained more pronounced effects of the different mutlipole transitions on the nuclear breakup cross section than on its Coulomb counterpart, for the $^{17}F + ^{208}Pb$ reaction. It is interesting to investigate whether similar conclusions can be drawn as well for reactions induced by neutron-halo projectiles.

In this work, we study the first- and higher-order interferences on the total (Coulomb+nuclear), Coulomb, and nuclear breakup cross sections, for the $^{15}C + ^{208}Pb$, $^{11}Be + ^{208}Pb$ reactions at 68 MeV/u, using the CDCC method. We aim especially to investigate how important are these interferences (i.e., their magnitudes and nature) on the total and nuclear breakup cross sections, for a better understanding of the nuclear breakup contribution on these two reactions and then testing the accuracy of excluding the nuclear breakup contribution when the different multipole breakup cross sections are summed incoherently, as is the case in the CD method.

The use of the CDCC method for such studies is motivated by the fact that both Coulomb and nuclear breakups are treated at the same footing. Multipole excitations are fully included as well as the final state interaction effects [21]. On the other hand, the choice of these two reactions is firstly justified by the availability of the experimental data, making the comparison

*bmukeru@gmail.com, mukerb@unisa.ac.za
†lekalml@unisa.ac.za

easy. Secondly, the two projectiles exhibit similar ground state configurations [27,28]. Furthermore, the ^{11}Be ground state binding energy is less than the one of the ^{15}C nucleus, thus providing an opportunity to assess the role of the ground state binding energy on our findings.

The methodology adopted in this paper consists of the following steps: first we perform first-order (FO) CDCC calculations, and estimate the first-order interference. Second, we estimate the all-order (AO) interference, where all the different multipoles retained in the CDCC model space are included coherently and incoherently. Finally, the higher-order interference is then estimated by considering the difference between the first-and all-order interferences. The numerical calculations are performed using the FRESCO codes [29].

This paper is structured as follows. In Sec. II, we briefly recall the main features of CDCC method, in Sec. III the results and discussion are presented, and Sec. IV is devoted to the conclusions.

II. BRIEF THEORETICAL DESCRIPTION

A brief summary of the important features of the CDCC method is presented here. More details can be found in Refs. [22,23,30–35]. In general, in this method, the projectile p is assumed to have a two-body structure, where a valence nucleon v is loosely bound to a core c, such that its breakup on a target t is treated as a three-body problem. The target is kept structureless, meaning that no explicit target excitations are taken into account, other than those due to projectile-target optical potentials.

The internal Hamiltonian H_p of the projectile is given by

$$H_p = -\frac{\hbar^2}{2\mu_{cv}}\frac{d^2}{dr^2} + V_{cv}(\mathbf{r}), \tag{1}$$

where μ_{cv} is the projectile reduced mass and $V_{cv}(\mathbf{r})$ the core-nucleon interacting potential. The continuum wave functions $[\phi^j_{k\ell}(r)]$ of the projectile are radial parts of H_p, normalized according to

$$\phi^j_{k\ell}(r\to\infty) \to F_\ell(kr)\cos\delta_{\ell j}(k) + G_\ell(kr)\sin\delta_{\ell j}(k), \tag{2}$$

where F_ℓ and G_ℓ are Coulomb functions [13] and $\delta_{\ell j}(k)$ the nuclear phase shifts.

Following [13,22,30], we adopt the binning technique and slice the continuum wave functions $\phi^j_{k\ell}(r)$ into bins of widths $\Delta k_i = k_i - k_{i-1}$ $(i = 1,2,\ldots,N_b$, with N_b the number of bins), averaged over the relative momentum (k). With this technique, one obtains discretized continuum wave functions, which are square integrable and given by [13,35]

$$\varphi_\alpha(r) = \sqrt{\frac{2}{\pi W_\alpha}}\int_{k_{i-1}}^{k_i} g_\alpha(k)\phi^j_{k\ell}(r)dk, \tag{3}$$

where $g_\alpha(k)$ is some weight function, and $W_i = \int_{k_{i-1}}^{k_i}|g_\alpha(k)|^2dk$ is a normalization coefficient. The subscript $\alpha = (i,\ell,s,j)$ represents the relevant quantum numbers describing the states of the projectile, where $i = 0$ refers to the ground state. In each bin, the bin energy is defined by

$$\varepsilon_\alpha = \frac{\hbar^2}{2\mu_{cv}W_\alpha}\int_{k_{i-1}}^{k_i} k^2 g_\alpha(k)dk. \tag{4}$$

The weight function $g_\alpha(k)$ depends on the state of the bins. For instance it is common to use $g_\alpha(k) = 1$, for non-S-wave nonresonant bins, which corresponds to $W_i = (\Delta k_i)^{1/2}$ and $\varepsilon_i = \frac{\hbar^2\hat{k}_i^2}{2\mu_{cv}}$, where $\hat{k}_i = (k_i^2 + k_{i-1}^2 + k_i k_{i-1})/3$. To stabilize the extraction of the three-body amplitude, it is convenient to use $g_\alpha(k) = k$ [30]. In the case of resonant bins, we adopt the prescription of [31].

Having constructed the bin wave functions, the three-body CDCC wave function can then be expanded as follows [13]:

$$\Psi^{\rm CDCC}_{\rm JM}(\mathbf{r},\mathbf{R}) = \frac{1}{rR}\sum_{\alpha,L}\chi^{LJ}_\alpha(R)[i^L\Phi_\alpha(\mathbf{r})\otimes Y_L(\hat{R})]_{JM}, \tag{5}$$

where

$$\Phi_\alpha(\mathbf{r}) = \varphi_\alpha(r)\left[i^\ell Y^{m_\ell}_\ell(\hat{r})\otimes X^{m_s}_s\right]_{jm}, \tag{6}$$

with $\varphi_\alpha(r)$ given by Eq. (3). The substitution of the expansion (5) into the three-body Schrödinger equation leads to a set of coupled equations for the coefficients χ^{LJ}_α, reading

$$\left[-\frac{\hbar^2}{2\mu_{pt}}\left(\frac{d^2}{dR^2} - \frac{L(L+1)}{R^2}\right) + V^{LJ}_{\alpha\alpha}(R) + \varepsilon_\alpha - E\right]\chi^{LJ}_\alpha(R) - \sum_{\alpha\neq\alpha'} i^{L-L'}V^{LL'J}_{\alpha\alpha'}(R)\chi^{L'J}_{\alpha'}(R) = 0, \tag{7}$$

where μ_{pt} is the projectile-target reduced mass, and $V^{LL'J}_{\alpha\alpha'}(R)$ the potential matrix element, coupling the ground state to continuum states as well as continuum to continuum states of the projectile, and has the following expression:

$$V^{LL'J}_{\alpha\alpha'}(R) = \langle\mathcal{Y}_{\alpha L}(\mathbf{r},\hat{R})|U_{ct} + U_{vt}|\mathcal{Y}_{\alpha' L'}(\mathbf{r},\hat{R})\rangle, \tag{8}$$

where

$$\mathcal{Y}_{\alpha L}(\mathbf{r},\hat{R}) = \left[i^L\hat{\Phi}_\alpha(\mathbf{r})\otimes Y_L(\hat{R})\right]_{JM}, \tag{9}$$

and U_{ct} and U_{vt} are the core-target and neutron-target phenomenological optical potentials, including nuclear and Coulomb components. They also account for the absorption from all the channels which are not included in the model space. The coupled equations (7) are solved with the usual boundary conditions at $R\to\infty$, which are

$$\chi^{LJ}_\alpha(R) \to \frac{i}{2}[H^-_\alpha(K_\alpha R)\delta_{\alpha\alpha'} - H^+_\alpha(K_\alpha R)S_{\alpha\alpha'}(R)], \tag{10}$$

where $H^\pm_\alpha(K_\alpha R)$ are Coulomb Hankel functions [13] and $S_{\alpha\alpha'}(K_\alpha)$ is the breakup S matrix, with $K_\alpha = \sqrt{\frac{2\mu_{pt}(E+\varepsilon_\alpha)}{\hbar^2}}$. The breakup observables are obtained from the breakup S matrix as described in [13,30].

III. RESULTS AND DISCUSSION

A. Projectile description and CDCC input parameters

We first describe the projectile structures and the CDCC model space parameters. Starting with the ^{15}C projectile, we consider the $^{14}\mathrm{C}\otimes n(2s_{\frac{1}{2}^+})$ ground state configuration,

TABLE I. Core-neutron potential parameters, taken from Ref. [38].

Core-neutron	$V_{\ell=0}$ (MeV)	$V_{\ell>0}$ (MeV)	V_{SO} (MeV fm^2)	a (fm)	R_0 (fm)
$n + {}^{10}$Be	59.5	40.5	32.8	0.6	2.699
$n + {}^{14}$C	52.814	51.3	20.77	0.6	2.959

as suggested in Refs. [27,36,37], with a binding energy of 1.218 MeV and parity $J^\pi = \frac{1}{2}^+$. Its first excited state has an excitation energy of 0.478 MeV and parity $J^\pi = \frac{5}{2}^+$. The $J^\pi = \frac{3}{2}^+$ partial wave contains a resonance of 3.56 ± 0.1 MeV [38]. For the ^{11}Be projectile on the other hand, we adopt the $^{10}\text{Be} \otimes n(2s_{\frac{1}{2}^+})$ ground state configuration as in Ref. [28], with a binding energy of 0.503 MeV and parity $J^\pi = \frac{1}{2}^+$. The first excited state has an excitation energy of 0.183 MeV, and parity $J^\pi = \frac{1}{2}^-$, and a narrow resonance of 1.274 ± 0.0018 MeV [39] is located in the $J^\pi = \frac{5}{2}^+$ partial wave. The ground, continuum, as well as resonant states of the projectiles are obtained by solving the corresponding Schrödinger equation using the core-neutron potential parameters listed in Table I. The projectile-target optical potential parameters used to calculate the potential matrix element are presented in Table II, whereas the CDCC model space parameters are summarized in Table III. These parameters are selected based on the convergence requirements. The energy interval $[0, \varepsilon_{max}]$ is discretized into bins of widths $\Delta\varepsilon_i = 0.5$ MeV for the s and p waves, $\Delta\varepsilon_i = 1$ MeV for the d and f waves, and $\Delta\varepsilon_i = 2$ MeV for the gwaves. We verified that the convergence of the results does not depend on a special discretization of the resonant states.

B. Energy distributions partial-wave analysis

Motivated by the contradicting results of Refs. [20,21], we first perform a partial-wave analysis for the two reactions to assess, on one hand, the contributions of the different partial waves included in the CDCC model space. On the other hand, we analyze the role of the nuclear breakup and the significance of the Coulomb-nuclear interference. The results obtained for the $^{15}\text{C} + {}^{208}\text{Pb}$ reaction are presented in Fig. 1. Concerning the partial-wave contributions, the results in Fig. 1(a) show, as expected, a large dominance of the p waves (down-pointing triangles) which also dictate the shape of the total breakup cross section (solid line). However, one sees that the contribution of the other partial waves is important,

TABLE II. Core-target and neutron-target optical potential parameters, taken from Ref. [38].

c/n + target	V (MeV)	W (MeV)	R_R (fm)	R_I (fm)	a_R (fm)	a_I (fm)
$^{10}\text{Be} + {}^{208}\text{Pb}$	70.00	58.90	7.43	7.19	1.04	1.00
$^{14}\text{C} + {}^{208}\text{Pb}$	70.00	58.90	7.67	7.42	1.04	1.00
$n + {}^{208}\text{Pb}$	29.46	13.40	6.93	7.47	0.75	0.58

TABLE III. CDCC model space parameters.

ℓ_{max} ($\hbar$)	λ_{max}	ε_{max} (MeV)	r_{max} (fm)	Δr (fm)	L_{max} ($\hbar$)	R_{max} (fm)	ΔR (fm)
4	4	9	60	0.1	10000	1000	0.005

since it is clear that $\sum_\ell \sigma_T^\ell < \sigma_T$ (where σ_T is the coherent sum of both the nuclear and Coulomb breakup cross sections). The g waves were found to be insignificant, and are therefore not plotted, although we checked that they are important in obtaining converged results. Our results are consistent with the findings of Ref. [21].

In order to analyze the role of the nuclear breakup contribution, we present in Fig. 1(b) the differential total (solid line), only Coulomb (diamonds), and only nuclear (up-pointing triangles) breakup cross sections. The results indicate that the nuclear breakup cross section is not negligible, especially at low excitation energies. Also it can be seen that the Coulomb breakup cross section largely overestimates the data and is more important than the total breakup cross section. The data are, however, well fitted by the total breakup cross section. A closer look at this figure shows that $\sigma_N < \sigma_T - \sigma_C$ (where σ_N and σ_C are the nuclear and Coulomb breakup cross sections, respectively). This inequality is an indication of the fact that a small nuclear contribution does not automatically imply

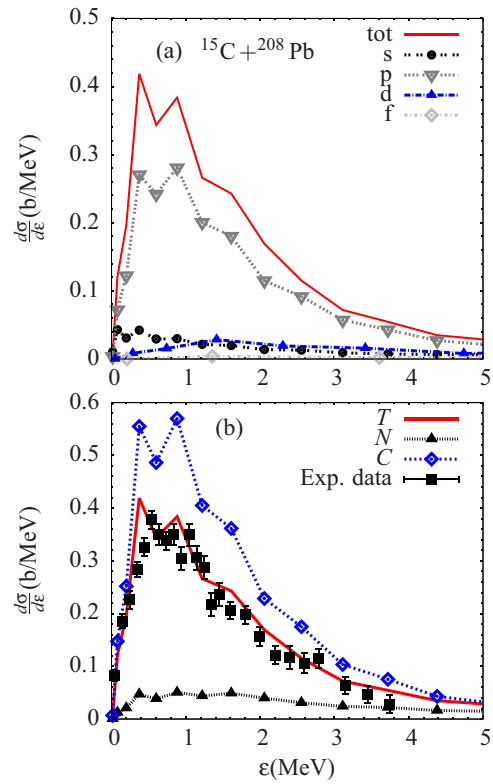

FIG. 1. (Color online) (a) Different partial-wave differential breakup cross sections; (b) total, Coulomb, and nuclear breakup cross sections for the $^{15}\text{C} + {}^{208}\text{Pb}$ reaction. See text for the details. The experimental data are taken from Ref. [37].

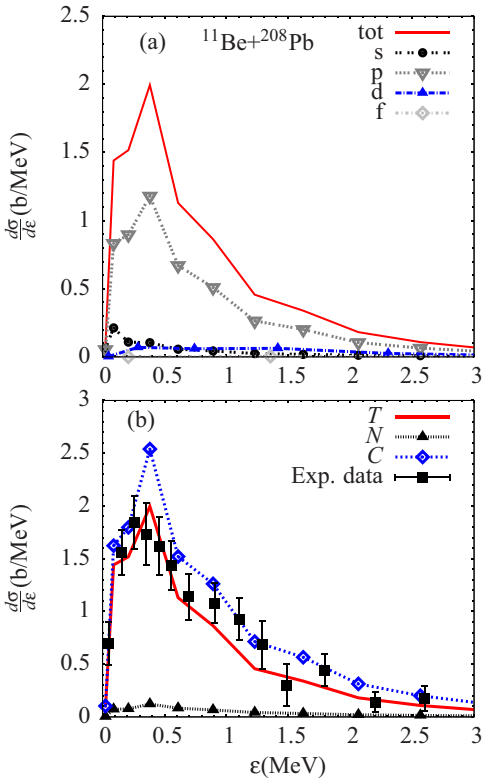

FIG. 2. (Color online) (a) Different partial-wave differential breakup cross sections; (b) total, Coulomb, and nuclear breakup cross sections for the $^{11}\mathrm{Be} + {}^{208}\mathrm{Pb}$ reaction. The experimental data are taken from Ref. [11].

small Coulomb-nuclear interference, which is destructive in this case.

We now turn to the $^{11}\mathrm{Be} + {}^{208}\mathrm{Pb}$ reaction, where the results are presented in Fig. 2. Looking at Fig. 2(a), where the partial breakup cross sections are shown, it is seen that, qualitatively, we can draw similar conclusions as for the $^{15}\mathrm{C} + {}^{208}\mathrm{Pb}$ reaction [see Fig. 1(a)]. However, quantitatively, here the partial breakup cross sections are much larger, which is not surprising given the lower ^{11}Be binding energy compared to the one of ^{15}C. We can then conclude that the importance of the p waves is not binding energy dependent, at least for these two reactions. Finally, in Fig. 2(b), the differential total, Coulomb, and nuclear breakup cross sections are presented. It is similarly observed that the Coulomb breakup cross section dominates over the total and fairly fits the data at high excitation energies. The results also show that although the nuclear breakup is quite small (and becomes even negligible at $\varepsilon \geqslant 1.5$ MeV), the Coulomb-nuclear interference is more significant and the total breakup cross section provides a good fit of the data at low excitation energies ($\varepsilon \leqslant 1$ MeV). Our results disagree with the prediction of Ref. [10], where it was pointed out that the disagreement between the data and the Coulomb dissociation method (mostly at high excitation energies) could be due to the nuclear breakup and/or higher-order effects. Rather, it could be due to the description of the reaction.

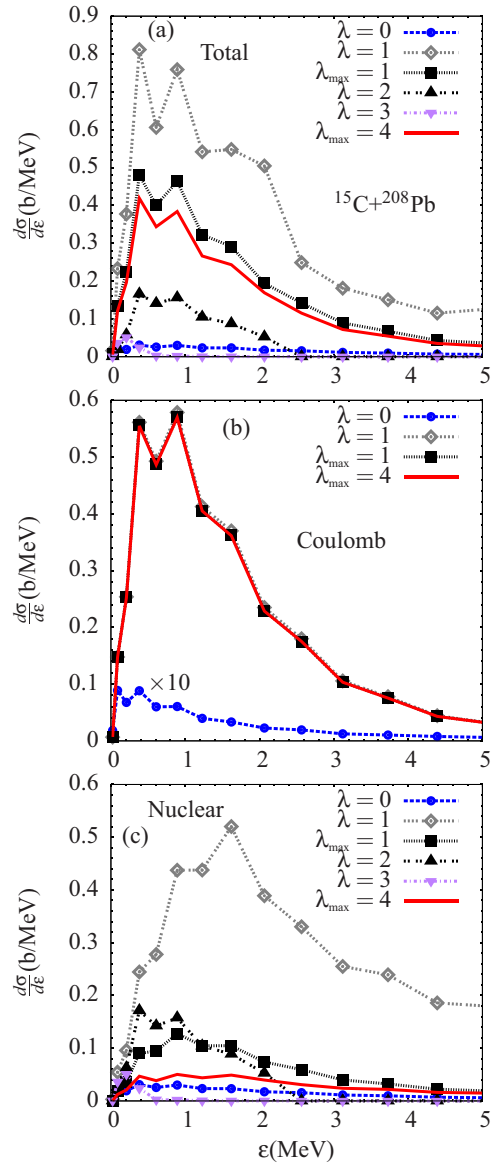

FIG. 3. (Color online) Energy-distribution differential (a) total, (b) Coulomb, and (c) nuclear breakup cross sections, corresponding to different multipoles, for the $^{15}\mathrm{C} + {}^{208}\mathrm{Pb}$ reaction. The different curves are explained in the text.

C. First- and higher-order interferences

In order to investigate the first- and higher-order interferences, we first analyze the importance of each single multipole transition. For each multipole, a partial-wave analysis is performed to assess how these partial waves are populated by the different multipole transitions. In what follows, $\lambda = a$ denotes a single multipole transition of value a, and $\lambda_{\max} = a$, stands for a coherent sum $\lambda = 0, \ldots, a$ and accounts for the multipole interference.

The energy-distribution differential breakup cross sections are presented in Fig. 3 for the $^{15}\mathrm{C} + {}^{208}\mathrm{Pb}$ reaction, and in Fig. 4 for the $^{11}\mathrm{Be} + {}^{208}\mathrm{Pb}$ reaction. Starting with the $^{15}\mathrm{C} + {}^{208}\mathrm{Pb}$ reaction, the total breakup cross sections presented in Fig. 3(a) show that the first-order [$\lambda = 1$ (diamonds)]

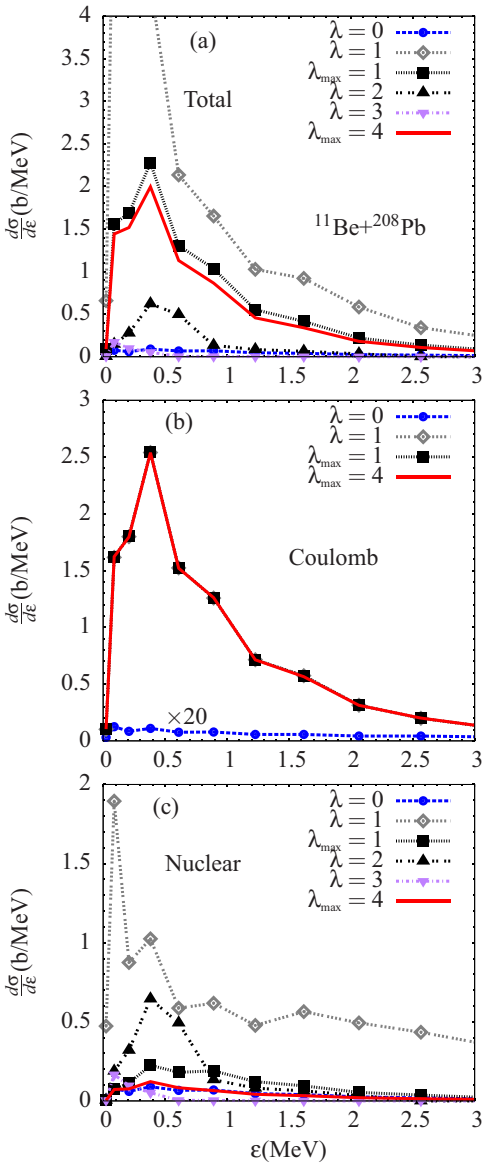

FIG. 4. (Color online) Energy-distribution differential (a) total, (b) Coulomb, and (c) nuclear breakup cross sections, corresponding to different multipoles, for the ^{11}Be + ^{208}Pb reaction.

cross section is significantly dominant, followed by the second-order [$\lambda = 2$ (up-pointing triangles)] cross section, whereas the third-order [$\lambda = 3$ (down-pointing triangles)] cross section is negligible for energies $\geqslant 0.5$ MeV. Compared to the first-order breakup cross section, the zero-order [$\lambda = 0$ (circles)] breakup cross section is insignificant. Surprisingly, the [$\lambda_{max} = 1$ (squares)] breakup cross section is much less than the first-order breakup cross section. This is a clear effect of the first-order ($\lambda = 0,1$) interference, which is seen to be strongly destructive. Including all the multipoles coherently, we find that the all-order [$\lambda_{max} = 4$ (solid line)] breakup cross section curve only differs from the $\lambda_{max} = 1$ curve for energies $0.5 \leqslant \varepsilon < 4$ MeV, in which interval the higher-order ($\lambda = 2,3$) effects are significant.

The Coulomb breakup cross sections presented in Fig. 3(b) indicate also a negligible $\lambda = 0$ breakup cross section (it is multiplied by 10 for convenience). Moreover, it can be seen that the first-order, the $\lambda_{max} = 1$, and the all-order breakup cross section curves are hardly distinguishable, showing that the first- and higher-order interferences are negligible. Therefore, the coherent and incoherent sums of the first- and all-order Coulomb breakup cross sections are not expected to be that different. Lastly, the nuclear breakup cross sections are presented in Fig. 3(c), where the results show that conclusions similar to those of Fig. 3(a) can be drawn. However, a much more destructive higher-order interference is noticed in this case.

For the ^{11}Be + ^{208}Pb reaction, the corresponding results given in Figs. 4(a), 4(b), and 4(c), for the total, Coulomb, and nuclear breakup cross sections, respectively, indicate that we can still reach conclusions similar to those for the ^{15}C + ^{208}Pb reaction, although here we observe larger breakup cross sections, due to the same reasons pointed out in Sec. III B.

For a quantitative analysis of the first- and higher-order interferences as well as the effects of the different multipoles on the Coulomb-nuclear interference, we integrate the different partial-wave differential breakup cross sections. The energy integrated breakup cross sections are presented in Table IV. In this table, $\sigma_C^\ell + \sigma_N^\ell$ represents the incoherent sum of the Coulomb and nuclear partial integrated breakup cross sections, while Δ_C^ℓ and Δ_N^ℓ (in %) stand for the contributions of both the Coulomb and nuclear partial breakup cross sections to their incoherent sums. The incoherent sum of the partial breakup cross sections ($S_i^\lambda, \lambda = i$) for each single multipole is defined as

$$S_i^\lambda = \sum_{\ell=0}^{\ell_{max}} \sigma_x^\ell, \quad x = C,N,T \tag{11}$$

and $S_i^{\lambda_{max}}$, $\lambda_{max} = i$ stands for the incoherent sum of the partial-wave breakup cross sections, when the different multipoles are included coherently.

Considering the different multipole transitions, the table shows that at zero order only transitions from the ground states to the s continuum states are accounted for. At first order, transitions to all s, p, d, f, and g continuum states are observed. At second order, only transitions to s, d, and g continuum states are noticed, where the d-wave breakup cross sections are more important. Finally, at third order, again transitions to all s, p, d, f, and g continuum states are possible, where f-wave breakup cross sections are more significant.

Comparing the Coulomb and nuclear contributions (7th, 8th, 13th, and 14th columns) to their incoherent sums, it can be seen that for each partial wave and each single multipole the nuclear breakup cross sections are more important than their Coulomb breakup counterparts (except for $\lambda = 1$ and for the ^{11}Be + ^{208}Pb reaction). More precisely, for the ^{15}C + ^{208}Pb reaction and for the Coulomb breakup, the table shows that $S_\lambda = S_0^\lambda + S_1^\lambda + S_2^\lambda + S_3^\lambda = 998.41$ mb, while $S_\lambda = 2135.03$ mb for the nuclear breakup. Looking at the ^{11}Be + ^{208}Pb reaction, we have that $S_\lambda = 2073.07$ mb for the Coulomb breakup and $S_\lambda = 3863.09$ mb for the nuclear breakup.

Considering the effects of the first- and all-order interferences, from the table one can observe a substantial reduction of

TABLE IV. Partial integrated breakup cross sections (in millibarns). The numerical integration is performed up to $\varepsilon_{\max} = 5$ MeV.

		$^{15}C + ^{208}Pb$						$^{11}Be + ^{208}Pb$					
		σ_T^ℓ	σ_C^ℓ	σ_N^ℓ	$\sigma_C^\ell + \sigma_N^\ell$	Δ_C^ℓ	Δ_N^ℓ	σ_T^ℓ	σ_C^ℓ	σ_N^ℓ	$\sigma_C^\ell + \sigma_N^\ell$	Δ_C^ℓ	Δ_N^ℓ
$\lambda = 0$	S_0^λ	80.84	14.03	80.84	94.87	14.80%	85.2%	145.80	12.43	145.80	158.22	7.86%	92.14%
	s	429.05	57.14	174.12	231.26	24.71%	75.29%	1263.02	226.82	415.51	642.33	35.31%	64.69%
	p	1110.44	833.70	1076.54	1910.24	43.64%	56.36%	2611.95	1560.40	1259.46	2819.856	55.34%	44.66%
$\lambda = 1$	d	380.45	86.16	182.19	268.35	32.11%	67.89%	824.60	166.93	407.17	574.10	29.08%	70.92%
	f	99.60	6.39	19.37	25.76	24.81%	75.19%	162.80	42.37	116.52	158.90	26.67%	73.33%
	g	15.73	0.54	0.76	1.30	41.47%	58.53%	41.076	15.67	36.83	52.50	29.85%	70.15%
	S_1^λ	2035.26	983.93	1452.97	2436.90	40.38%	59.62%	4903.45	2012.20	2235.48	4247.69	47.37%	52.63%
	s	105.79	0.00	112.47	112.47	0.00%	100%	161.82	13.06	176.03	189.09	06.91%	93.09%
	p	0.00	0.00	0.00	0.00	0.00%	0.00%	0.00	0.00	0.00	0.00	0.00%	0.00%
$\lambda = 2$	d	323.93	0.45	329.52	329.96	0.13%	99.87%	858.15	23.41	889.11	912.52	2.56 %	97.44%
	f	0.00	0.00	0.00	0.00	0.00%	0.00 %	0.00	0.00	0.00	0.00	0.00%	0.00%
	g	12.93	0.00	14.46	14.46	0.00%	100%	48.21	5.18	51.94	57.12	09.06%	90.94%
	S_2^λ	442.65	0.45	456.44	456.90	0.10%	99.90%	1068.18	41.64	1117.08	1158.72	3.59%	96.41
	s	18.48	0.00	18.36	18.36	0.00%	100%	44.93	1.36	42.21	42.57	3.13%	96.87%
	p	0.16	0.00	0.16	0.16	0.00%	100%	0.46	0.03	0.37	0.40	7.90%	92.10%
$\lambda = 3$	d	4.56	0.00	4.55	4.55	0.00%	100%	10.20	0.21	10.44	10.65	1.98%	89.02%
	f	119.97	0.00	119.66	119.66	0.00%	100%	309.38	4.79	304.92	309.71	1.55%	98.45%
	g	2.07	0.00	2.05	2.05	0.00%	100%	8.55	0.40	6.79	7.19	5.56%	94.44%
	S_3^λ	145.24	0.00	144.78	144.78	0.0%	100%	373.52	6.80	364.73	371.53	1.83%	98.17%
	s	184.05	61.85	58.12	119.97	51.55%	48.45%	337.43	225.90	96.84	322.74	70.00%	30.00%
	p	667.32	819.16	213.11	1032.27	79.36%	20.64%	1297.31	1559.57	209.20	1768.77	88.17%	11.83%
$\lambda_{\max} = 1$	d	106.91	83.52	28.17	111.69	74.78%	25.22%	157.02	168.85	22.03	190.88	88.46%	11.54%
	f	19.25	6.41	0.08	6.49	98.75%	1.25%	28.64	44.67	1.22	45.89	97.33%	2.67%
	g	2.60	0.58	0.08	0.66	87.65%	12.35%	3.00	17.44	0.048	17.49	99.73%	0.27%
	$S_1^{\lambda_{\max}}$	980.13	971.52	299.57	1271.09	76.43%	23.57%	1823.39	2016.43	329.33	2345.76	85.96%	14.04%
	s	79.64	62.08	22.27	84.35	73.60%	26.40%	121.37	221.77	30.96	252.73	87.77%	12.23%
	p	563.75	818.25	105.10	923.35	88.62%	11.38%	1092.85	1558.67	69.48	1628.15	95.73%	4.27%
$\lambda_{\max} = 4$	d	80.81	82.50	22.79	105.28	78.35%	21.65%	148.23	168.14	65.37	233.51	72.01%	27.99%
	f	13.01	6.41	8.89	15.29	41.92%	58.08%	14.67	44.91	23.75	68.66	65.41%	34.59%
	g	6.50	0.61	4.16	4.78	12.69%	87.31%	18.54	15.87	12.92	28.79	53.13%	44.87%
	$S_4^{\lambda_{\max}}$	743.71	969.83	163.20	1133.03	85.60%	14.40%	1395.66	2009.36	202.46	2211.82	90.85%	09.15%

the nuclear breakup cross sections, which become negligible compared to the Coulomb breakup cross sections for both reactions. A close look at the $S_1^{\lambda_{\max}}$ and $S_4^{\lambda_{\max}}$ sums reveals that this substantial reduction of the nuclear breakup cross section is largely due to the first-order interference. It is also noticed that the dominance of the Coulomb breakup cross section over the total is an effect of the first-order interference for the $^{11}Be + ^{208}Pb$ reaction, and of the higher-order interference for the $^{15}C + ^{208}Pb$ reaction.

In order to get a better quantitative understanding of the first- and higher-order interferences, we present in Table V, the amounts (in percentage) reduced from the different breakup cross sections due to the first-order interference (σ_I^{FO}) and to the all-order interference (σ_I^{AO}), defined as

$$\sigma_I^{FO} = 1 - \frac{S_1^{\lambda_{\max}}}{S_\lambda}, \quad \sigma_I^{AO} = 1 - \frac{S_4^{\lambda_{\max}}}{S_\lambda}. \tag{12}$$

The higher-order interference effect is then estimated by FO-AO. For the $^{15}C + ^{208}Pb$ reaction, it can be observed from the table that the all-order interference reduces by 72.50% the total breakup cross section, distributed as follows: 63.75% due to the first-order interference and 8.74% to the higher-order interference. It reduces the Coulomb breakup cross section by 2.86%, in the following distribution: 2.69% due to the first-order interference and 0.17% to the higher-order interference. For the nuclear breakup on the other hand, this interference reduces by 92.36% the breakup cross section, where 85.97% is due to the first-order interference and 6.39% to the higher-order interference. Our results for the $S_4^{\lambda_{\max}}$, and for the total breakup cross section, agree fairly with the 767 mb value of Ref. [40].

Finally, for the $^{11}Be + ^{208}Pb$ reaction, the results show that the reduction of the total breakup cross section due to the all-order interference amounts to 78.50%, distributed as follows: 71.91% due to the first-order interference and 6.59% to the higher-order interference. Looking at the Coulomb breakup cross section, a slight reduction of 3.07%, where 2.73% is due to the first-order interference and 0.34% to the higher-order interference, is noticed. As for the nuclear breakup cross section, one sees that the all-order interference reduces 94.76%, where 91.47% is due to the first-order interference and 3.29% to the higher-order interference.

TABLE V. First- and higher-order interference effects. FO (first-order), AO (all-order).

	$^{15}C + ^{208}Pb$						$^{11}Be + ^{208}Pb$					
		FO		AO				FO		AO		
	S_λ	$S_1^{\lambda_{max}}$	σ_I^{FO}	$S_4^{\lambda_{max}}$	σ_I^{AO}	FO-AO	S_λ	$S_1^{\lambda_{max}}$	σ_I^{FO}	$S_4^{\lambda_{max}}$	σ_I^{AO}	FO-AO
Tot.	2704.00	980.13	63.75%	743.71	72.50%	236.42(8.74%)	6490.95	1823.39	71.91%	1395.66	78.50%	427.73(6.59%)
Coul.	998.41	971.52	2.69%	969.83	2.86%	1.69(0.17%)	2073.07	2016.43	2.73%	2009.36	3.07%	7.07(0.34%)
Nucl.	2135.03	299.57	85.97%	163.20	92.36%	136.37(6.39%)	3863.09	329.33	91.47%	202.46	94.76%	126.87(3.29%)

The results show that, for the two reactions, the higher orders have small (<10%) effects on the integrated total, Coulomb, and nuclear breakup cross sections, while the total and nuclear breakup cross sections are substantially reduced at first order. However, the results in Figs. 1(b), 2(b), 3(a), and 4(a) indicate that the first-order differential breakup cross sections alone overestimate the data mostly at low excitation energies. Therefore, higher-order effects are also important in the analysis of these reactions.

Based on these results, it can be deduced that the dominance of the differential Coulomb breakup cross section over the total breakup cross section observed in Sec. III B, and in other works (for instance in Refs. [19,21]), is slightly due to the higher-order effects for the $^{15}C + ^{208}Pb$ reaction and to the first-order effects for the $^{11}Be + ^{208}Pb$ reaction. Moreover, it is clear that if the integrated breakup cross sections corresponding to the different multipoles were to be summed incoherently, the nuclear breakup cross section would largely prevail over the Coulomb breakup cross section even at first order. In such case, the elimination of the nuclear breakup contribution for obtaining the pure Coulomb breakup cross section would lead to more concerns regarding the accuracy of the obtained results. Our conclusions are in line with the ones drawn in Ref. [24] for the ^{17}F proton-halo projectile.

If we compare Figs. 1(b) and 2(b) with Figs. 6 and 7 of Ref. [38], it can be seen that our results are only qualitatively different from the results of this reference, where smooth curves scaled by a factor 0.85 are observed. To obtain smooth curves as in this reference, one can use for example the folding procedure adopted in Refs. [37,40], without affecting the conclusions.

So far, we have been discussing the energy-distribution breakup cross sections. However, to further get a clear understanding of the multipole transition effects on the three different breakups, as in Ref. [24], we also consider the angular-distribution breakup cross sections. The results are presented in Fig. 5, for the $^{15}C + ^{208}Pb$ reaction and in Fig. 6, for the $^{11}Be + ^{208}Pb$ reaction. In Fig. 5(a), it can be seen that the non-first-order differential total breakup cross sections are all negligible for $\theta \leqslant 2^\circ$, and the first-order breakup cross section is much extended to large angles. It is observed that, although the zero-order breakup cross section is negligible compared to the first-order breakup cross section, the first-order interference plays a significant role as it increases the $\lambda_{max} = 1$ breakup cross section at angles between 1° and 3.5°, before dropping systematically beyond 3.5°. Moreover, the results show that the all-order interference lowers the total breakup cross section at the whole range of angles, starting around 2°.

Considering the Coulomb breakup cross sections [Fig. 5(b)], one finds that the zero-order breakup cross section is negligible (the multiplication by 10 is again for convenience), while the first-order interference is more dominant and is responsible for the oscillatory behavior of the Coulomb

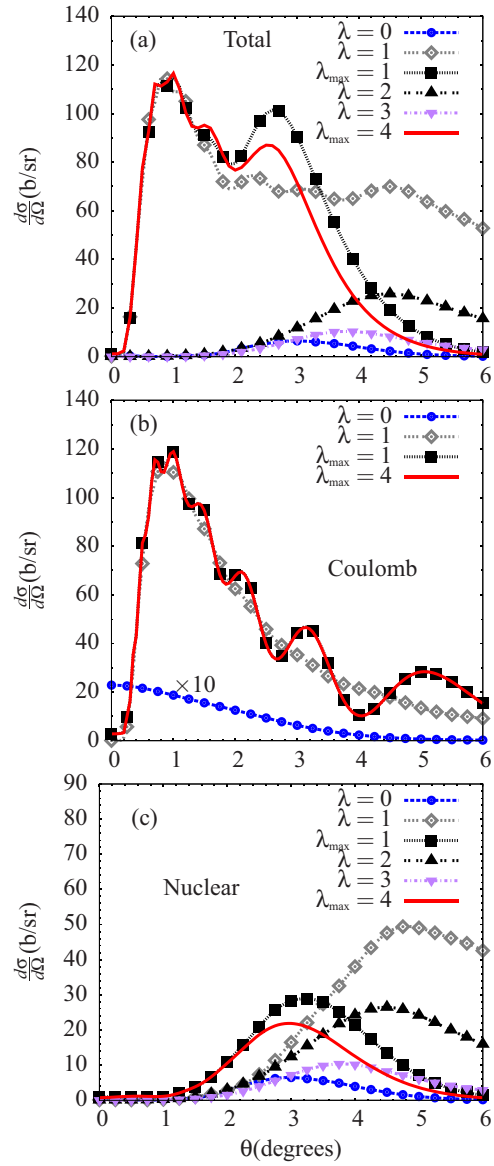

FIG. 5. (Color online) Angular-distribution differential (a) total, (b) Coulomb, and (c) nuclear breakup cross sections, corresponding to different multipoles for the $^{15}C + ^{208}Pb$ reaction.

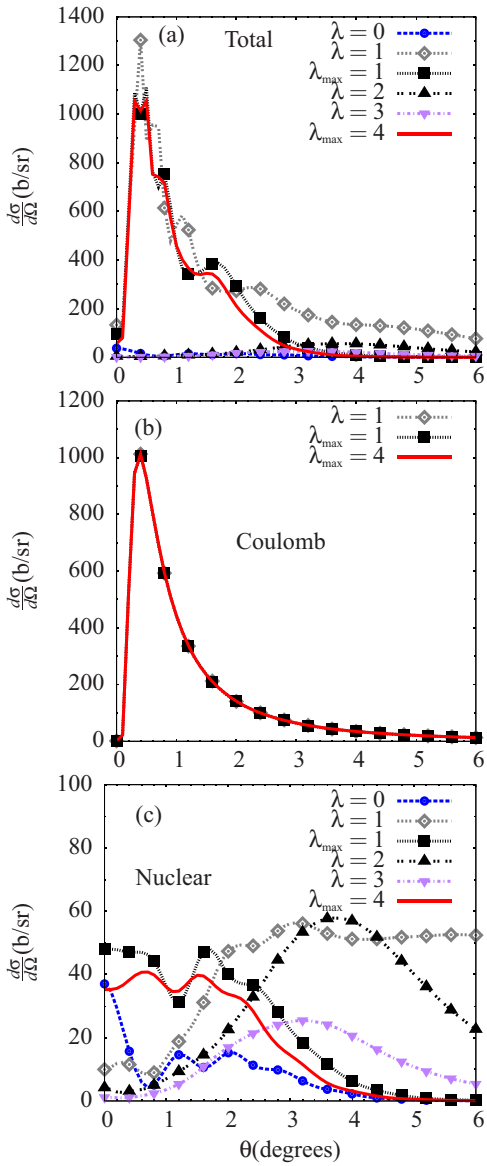

FIG. 6. (Color online) Angular-distribution differential (a) total, (b) Coulomb, (c) nuclear breakup cross sections, corresponding to different multipoles for the ^{11}Be + ^{208}Pb reaction.

breakup cross section. Lastly, Fig. 5(c) shows that all the nuclear breakup cross sections are negligible at $\theta \leqslant 1^\circ$, while the first-order breakup cross section is much extended at larger angles. Looking at Figs. 5(a) and 5(c), it is seen that both total and nuclear breakup cross sections exhibit some similarities regarding the effects of the first- and all-order interferences.

These results show that the oscillatory behavior observed in Fig. 5(a) is due to the first-order interference in the Coulomb breakup cross section. In Ref. [41], this oscillatory behavior was attributed to the nuclear breakup for the ^{8}B + ^{208}Pb reaction. Comparing our results to those obtained in Ref. [42], we find that in our case the oscillations are less pronounced. We can attribute the slight difference to the different projectile-target interactions employed in both works. Furthermore, a closer look at Figs. 5(b) and 5(c), shows as well that, if we were to perform an angular integration, the non-first-order integrated nuclear breakup cross sections would be more important than their Coulomb breakup counterparts.

Turning to the ^{11}Be + ^{208}Pb reaction, the results in Fig. 6(a) indicate again that we can still reach similar conclusions as in Fig. 5(a). However, in this figure one observes more oscillations and the first-order total breakup cross sections is less extended to larger angles. On the other hand, as expected, the total breakup cross sections in Fig. 5(a) are much less than in this figure, but by almost a factor 10.

For the Coulomb breakup [Fig. 6(b)], the results show that the $\lambda = 1$, $\lambda_{\max} = 1$, and $\lambda_{\max} = 4$ breakup cross section curves are also hardly distinguishable. It means that the non-first-order cross sections are insignificant and are therefore not plotted. From this figure one notices that the $\lambda_{\max} = 1$ curve does not exhibit the oscillatory pattern observed in Fig. 5(b). This indicates a qualitative difference between the Coulomb breakups of the two reactions. As for the nuclear breakup cross sections [Fig. 6(c)], it is seen that only higher-order breakup cross sections do not present oscillatory patterns; they are negligible at $\theta \leqslant 1^\circ$, but become important at backward angles. From the same figure, we also notice similar magnitudes at 0° for both the zero- and all-order nuclear breakup cross sections, and are as well hardly distinguishable at $\theta \geqslant 4^\circ$. These results show that the oscillations observed for the total breakup cross sections are due to the nuclear breakup component, in contrast to the ^{15}C + ^{208}Pb reaction.

The results in Figs. 5(c) and 6(c) also show that if the incoherent sum of $\lambda = 0,1$ angular integrated breakup cross section were considered, the incoherent nuclear sum would be more important than the Coulomb incoherent sum. These figures also show that in such cases the nuclear breakup contribution cannot be eliminated by any impact parameter value, as was the case in Ref. [11], since the nuclear contribution is important even at large angles, where one should expect negligible nuclear breakup cross sections due the nuclear absorption at small impact parameters.

IV. CONCLUSIONS

In this work, the first- and higher-order interference effects have been investigated for the ^{15}C + ^{208}Pb and ^{11}Be + ^{208}Pb reactions. The partial-wave analysis was first performed in order to check the importance of each partial wave included in the CDCC model space. It is shown that the p waves are more dominant for both reactions. But considered alone, they largely underestimate the data, hence the importance of the contributions of the other partial waves.

The total, Coulomb and nuclear breakups were analyzed separately. Comparing the results with the data, we found that for the ^{15}C + ^{208}Pb reaction the differential total breakup cross section fits the data well, while they are significantly overestimated by the differential Coulomb breakup cross section at the whole energy spectrum considered. This fitness was found to be an effect of the Coulomb-nuclear interference, which indicates that in this reaction the nuclear breakup contribution cannot simply be ignored. For the ^{11}Be + ^{208}Pb reaction, however, we observed that the total differential breakup cross section fits the data well at low excitation energies ($\varepsilon \leqslant 0.5$ MeV). However, the Coulomb differential

breakup cross section provided a fair fit of the data at high excitation energies. We then concluded that the disagreement observed between the data and the theory at high excitation energies in [10] could not be attributed to the nuclear and/or higher-order effects as predicted in that reference.

To analyze the first-order interference effects, we performed the first-order CDCC calculations by selecting single $\lambda = 0,1$ multipoles and their coherent sum $\lambda_{max} = 1$. We showed that when the two multipoles are summed incoherently, the integrated nuclear breakup cross section and hence the integrated total breakup cross section are much larger than the integrated Coulomb breakup cross section. However, the coherent sum indicated that the integrated nuclear breakup cross section is negligible compared to the integrated Coulomb breakup cross section, which becomes more important than its total breakup counterpart, due largely to the first-order interference. The conclusion was that this interference could be the reason why the total breakup cross section was found to be less than the Coulomb breakup cross section, not only in this study but also in [19,21] for the $^{19}C + ^{208}Pb$ and $^{15}C + ^{208}Pb$ reactions, respectively. These conclusions are valid even for angular-distribution breakup cross sections.

In order to study the higher-order interference effects, we first considered the all-order interference, which was taken care of by $\lambda_{max} = 4$. Then the higher-order interference was estimated using the first- and all-order interferences. For the $^{15}C + ^{208}Pb$ reaction, we obtained the following results. The all-order interference reduces by 72.50% the total breakup cross section, distributed as follows: 63.75% due to the first-order interference and 8.74% to the higher-order interference. It reduces by 2.86% the Coulomb breakup cross section, where 2.69% is due to the first-order interference and 0.17% to the higher-order interference. For the nuclear breakup cross section on the other hand, it is reduced by 92.36%, with 85.97% due to the first-order interference and 6.39% to the higher-order interference.

Concerning the $^{11}Be + ^{208}Pb$ reaction, 78.50% of the total breakup cross section is reduced due to the all-order interference, in the following distribution: 71.91% due to the first-order interference and 6.59% to the higher-order interference. The Coulomb breakup cross section is reduced by 3.07%, where 2.73% is due to the first-order interference and 0.34% to the higher-order interference. Finally, the all-order interference reduces by 94.76% the nuclear breakup cross section, distributed as follows: 91.47% due to the first-order interference and 3.29% to the higher-order interference.

Although the higher-order effects fall below 10% for both total and nuclear breakup cross sections, the results showed that the first-order results alone overestimate the data at low excitation energies and hence the importance of the higher-order interference effects, especially at low excitation energies.

ACKNOWLEDGMENTS

We would like to thank Prof. I. J. Thompson and Prof. D. Baye for useful discussions, especially for the numerical codes.

[1] G. Baur, K. Hencken, and D. Trautmann, Prog. Part. Nucl. Phys. **51**, 487 (2003).
[2] C. A. Bertulani and G. Baur, Phys. Rep. **163**, 299 (1988).
[3] G. Baur and H. Rebel, Annu. Rev. Nucl. Part. Sci. **46**, 321 (1996).
[4] C. Nociforo *et al.*, Phys. Lett. B **605**, 79 (2005).
[5] T. Aumann and T. Nakamura, Phys. Scr., **T152**, 014012 (2013).
[6] T. Nakamura *et al.*, Phys. Rev. Lett. **103**, 262501 (2009).
[7] S. Typel and G. Baur, Phys. Rev. C **64**, 024601 (2001).
[8] B. Abu-Ibrahim and Y. Suzuki, Progr. Theor. Phys. **112**, 1013 (2004).
[9] T. Nakamura *et al.*, Phys. Rev. Lett. **83**, 1112 (1999).
[10] N. Fukuda *et al.*, Phys. Rev. C **70**, 054606 (2004).
[11] N. Fukuda *et al.*, Progr. Theor. Phys. Suppl. **146**, 462 (2002).
[12] M. S. Hussein *et al.*, Phys. Lett. B **640**, 91 (2006).
[13] I. J. Thompson and F. M. Nunes, *Nuclear Reactions for Astrophysics* (Cambridge University Press, New York, 2009).
[14] K. Yoshida *et al.*, Prog. Theor. Phys. **053D03**, 1 (2014).
[15] R. Chatterjee and R. Shyam, Phys. Rev. C **66**, 061601(R) (2002).
[16] R. Chatterjee, Phys. Rev. C **75**, 064604 (2007).
[17] R. Chatterjee, Phys. Rev. C **68**, 044604 (2003).
[18] T. Tarutina and M. S. Hussein, Phys. Rev. C **70**, 034603 (2004).
[19] B. Mukeru, M. L. Lekala, and A. S. Denikin, J. Phys. G: Nucl. Part. Phys. **42**, 015109 (2015).
[20] A. Harvath *et al.*, Astrophys. J. **570**, 926 (2002).
[21] N. C. Summers and F. M. Nunes, Phys. Rev. C **78**, 011601(R) (2008).
[22] N. Austern *et al.*, Phys. Rep. **154**, 125 (1987).
[23] Y. Iseri *et al.*, Progr. Theor. Phys. Suppl. **89**, 84 (1986).
[24] Y. Kucuk and A. M. Moro, Phys. Rev. C **86**, 034601 (2012).
[25] J. F. Liang *et al.*, Phys. Lett. B **681**, 22 (2009).
[26] C. A. Bertulani and P. Danielewicz, Nucl. Phys. A **717**, 199 (2003).
[27] E. Sauvan *et al.*, Phys. Lett. B **491**, 1 (2000).
[28] S. Typel and R. Shyam, Phys. Rev. C **64**, 024605 (2001).
[29] www.fresco.org.uk
[30] J. A. Tostevin, F. M. Nunes, and I. J. Thompson, Phys. Rev. C **63**, 024617 (2001).
[31] T. Matsumoto, T. Kamizato, K. Ogata, Y. Iseri, E. Hiyama, M. Kamimura, and M. Yahiro, Phys. Rev. C **68**, 064607 (2003).
[32] R. A. D. Piyadasa, M. Kawai, M. Kamimura, and M. Yahiro, Phys. Rev. C **60**, 044611 (1999).
[33] T. Egami, K. Ogata, T. Matsumoto, Y. Iseri, M. Kamimura, and M. Yahiro, Phys. Rev. C **70**, 047604 (2004).
[34] I. J. Thompson and A. R. Barnett, J. Comput. Phys. **64**, 490 (1986).
[35] F. M. Nunes *et al.*, Nucl. Phys. A **736**, 255 (2004).
[36] D. Bazin, W. Benenson, B. A. Brown, J. Brown, B. Davids, M. Fauerbach, P. G. Hansen, P. Mantica, D. J. Morrissey, C. F. Powell, B. M. Sherrill, and M. Steiner, Phys. Rev. C **57**, 2156 (1998).
[37] T. Nakamura *et al.*, Phys. Rev. C **79**, 035805 (2009).
[38] P. Capel, D. Baye, and V. S. Melezhik, Phys. Rev. C **68**, 014612 (2003).
[39] P. Capel, G. Goldstein, and D. Baye, Phys. Rev. C **70**, 064605 (2004).
[40] H. Esbensen, Phys. Rev. C **80**, 024608 (2009).
[41] G. Goldstein, P. Capel, and D. Baye, Phys. Rev. C **76**, 024608 (2007).
[42] P. Capel, H. Esbensen, and F. M. Nunes, Phys. Rev. C **85**, 044604 (2012).